Analysis of the plasma transport in numerical simulations of helicon plasma thrusters

Cite as: AIP Advances **11**, 115016 (2021); https://doi.org/10.1063/5.0066221
Submitted: 09 August 2021 • Accepted: 22 October 2021 • Published Online: 08 November 2021

N. Souhair, M. Magarotto, F. Ponti, et al.

Analysis of the plasma transport in numerical simulations of helicon plasma thrusters

Cite as: AIP Advances 11, 115016 (2021); doi: 10.1063/5.0066221
Submitted: 9 August 2021 • Accepted: 22 October 2021 •
Published Online: 8 November 2021

N. Souhair,[1,a] M. Magarotto,[2,b] F. Ponti,[1,c] and D. Pavarin[2,d]

AFFILIATIONS

[1] Alma Propulsion Laboratory, Department of Industrial Engineering, University of Bologna, Forlì 47122, Italy
[2] Department of Industrial Engineering (DII), University of Padova, Padova 35131, Italy

[a] **Author to whom correspondence should be addressed:** nabil.souhair2@unibo.it
[b] **Electronic mail:** mirko.magarotto@unipd.it
[c] **Electronic mail:** fabrizio.ponti@unibo.it
[d] **Electronic mail:** daniele.pavarin@unipd.it

ABSTRACT

The accurate simulation of the plasma transport in helicon sources is a key aspect to improve the design of Helicon Plasma Thrusters (HPTs). Specifically, the 3D-VIRTUS code was proven to provide satisfactory estimations of the propulsive performance of realistic HPTs (difference between measures and numerical estimations of the thrust <30%). Nonetheless, further investigations are needed to deepen the influence that the plasma chemistry model, the formulation of the energy equation, and the definition of the diffusion coefficients have on the results of the simulation. First, a quantitative analysis has been conducted on a simplified configuration of HPT to study each phenomenon separately. Second, the generalized fluid model has been benchmarked against measures of plasma density performed on a helicon source. The radiative decay reactions affect the estimation of the performance (e.g., thrust) up to 40%. The quasi-isotherm formulation of the energy equation affects results (e.g., electron density) up to 30%. Accounting for anomalous transport or defining diffusion coefficients classically does not have a major effect on the simulation (e.g., thrust varies less than 20%). The generalized formulation of the fluid model provides estimations of the plasma density, which are within the uncertainty band of the measures (i.e., differences <20%).

I. INTRODUCTION

Plasma based electric propulsion has gained a great deal of interest in recent years mainly because of the high specific impulse achievable (up to 10 000 s).[1] Moreover, chemical rockets present an intrinsic limit in the energy available to produce thrust, which is stored in the chemical bonds of the propellant.[2] Conversely, electric propulsion systems are limited only by the amount of the power available on-board to operate the thruster.[1] One of the most promising concepts of the plasma propulsion system under development is the Helicon Plasma Thruster (HPT).[3] Referring to Fig. 1, two main stages can be distinguished in a HPT: the production stage in correspondence of the plasma source and the acceleration stage (or the "plume" stage) downstream the exhaust section of the thruster. Plasma is produced by introducing a mass flow of gaseous propellant into a helicon reactor.[4] This consists of a dielectric tube surrounded by a Radio Frequency (RF) antenna working in the MHz range.[5,6] Permanent magnets or coils are wrapped around the tube in order to provide a quasi-axial magnetic field that allows the propagation of helicon waves and enhances the confinement of the plasma inside the source.[7,8] The magnetic field also largely influences the acceleration stage providing the "magnetic nozzle" effect downstream the exhaust section of the thruster.[9] In a HPT, the stream of exhausted particles is a quasi-neutral and current-free plasma;[10] therefore, the system does not need grids, electrodes, and neutralizers like in traditional electric propulsion devices.[11] For this reason, HPTs are considered a cost-effective alternative particularly suitable for applications such as SmallSats and CubeSats.[5,6] Moreover, thanks to their simple design, HPTs can be operated with various propellants.[6,12,13] In synthesis, the HPT concept is simple from an engineering and a manufacturing point of view and versatile and with a virtually endless operational lifetime.[3]

The first research on HPTs was carried out by West *et al.* and the space plasma propulsion group at the Australian National University in the early 2000s.[14] Afterward, the HPT technology has been developed at the University of Padova during several projects, such

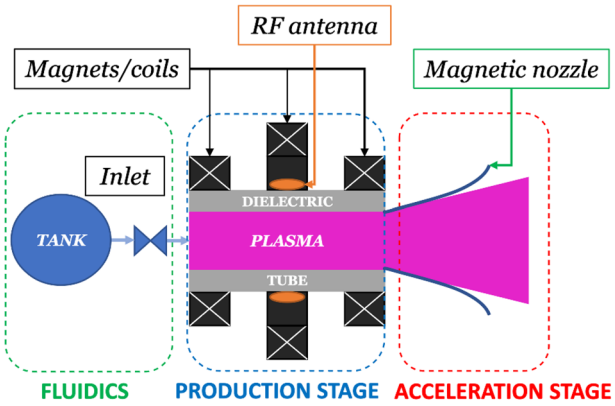

FIG. 1. Schematics of a helicon plasma thruster.[24]

as the European HPH.COM[15] and the Italian SAPERE/STRONG.[16] The outcomes of these two projects allowed the realization of REGULUS,[5,6] a propulsion unit developed by T4i[17] for CubeSats larger than 6U and SmallSats. The VASIMR rocket, developed by NASA, is another case of a propulsive system that employs a helicon source for the production stage.[18] The University of Madrid, along with SENER Aeroespacial, is designing and testing a 1 kW thruster as part of the HIPATIA project,[19] while the University of Stuttgart and the University of Manchester have been working on an atmosphere-breathing HPT to be used in Very Low Earth Orbits (VLEOs).[12] The research underway at Tohoku University in Japan is also shedding light on the physical mechanisms and plasma behavior that govern the performance of HPTs, allowing for their optimization.[20] The Massachusetts Institute of Technology,[21] the Michigan Institute of Technology,[22] and Washington University[23] have also worked on and contributed to the HPT technology.

When it comes to optimizing the design of a HPT, it is fundamental to simulate in an accurate manner the plasma dynamics. In this regard, the development of numerical tools is required to grasp all the physical phenomena governing a HPT.[3] Many numerical methods have been used in the literature for modeling the plasma production and acceleration; the most important approaches are the fluid,[9,25] kinetic,[10,26,27] Particle-In-Cell with Monte-Carlo Collisions (PIC-MCC),[28,29] and hybrid.[30–32] The fluid approach assumes the particle distribution function to describe the plasma in terms of continuity, momentum, and energy equations.[33] This method is less demanding in terms of computational resources and thus is widely used.[34] The fluid approach shows, though, to be limited whenever the particle distribution function departs significantly from the equilibrium (i.e., the Maxwellian), e.g., when diluted and weakly collisional plasma is considered.[30] The kinetic approach is based on the Boltzmann equation together with the solution of the Maxwell equations[33] and determines uniquely the self-consistent particle distribution function, which is then linked to the macroscopic fluid properties of interest (e.g., density, temperature, and mean velocity) by its averaging.[33] This method is usually exploited under simplified hypotheses (e.g., mono-dimensional domain) to limit the computational burden.[26,34] The PIC-MCC approach integrates in an accurate manner the particle trajectories under the effect of Electro-Magnetic (EM) fields,[28] which makes the method particularly suitable for the investigation of non-equilibrium situations. Even though very accurate, this method is computationally intensive, especially for a high density plasma (e.g., $>10^{19}$ m^{-3}).[30] Finally, to preserve the accuracy of kinetic and PIC-MCC methods, while reducing the computational burden, the approaches mentioned above have been combined in hybrid solvers.[30,32,35] In this regard, it is worth mentioning the Hyphen code developed at the University of Madrid in which the hybrid solution of the plasma motion is coupled to an EM module in order to obtain a self-consistent description of HPTs[31] and/or Electron Cyclotron Resonance (ECR) thrusters.[32] With Hyphen, the plasma dynamics is solved both in the source and in part of the plume.

Recently, a promising numerical tool has been developed at the University of Padova, namely, 3D-VIRTUS,[36] to simulate the production stage of a HPT. Specifically, this tool is composed of two mutually coupled modules: the first one solves the EM wave propagation and thus the power coupled into the plasma by the antenna;[37] the second is a fluid module that handles the plasma transport.[36] The latter relies on the finite-volume method and has been implemented via the OpenFOAM library.[38] It comprises, for each plasma species (i.e., electrons, ions, neutrals and excited), a set of governing equations based on the Drift-Diffusion (DD) approximation.[36] Considering that the wave propagation has faster dynamics compared to the plasma transport (at least three orders of magnitude[36]), the two phenomena are solved individually in an iterative loop until convergence. 3D-VIRTUS can be used to estimate the propulsive performance (e.g., thrust and specific impulse) of a HPT if coupled with a tool that solves the acceleration stage. To this end, a simplified analytical model[39] has been adopted, providing a satisfactory estimation of the performance of a real HPT, being the maximum disagreement between predictions and measures of the thrust lower than 30%.[7] Even though this strategy has proven to give promising results, improvements are needed mainly for what the simulation of the acceleration stage is concerned[40] but also in terms of the diffusion model implemented for the solution of the production stage. The latter aspect has been addressed in this paper for what the plasma chemistry,[41] the energy equation,[42] and the anomalous diffusion[43] are concerned. Considering an argon based plasma, the chemistry model has been improved with a set of reactions for the $3p^5 4s$ and $3p^5 4p$ (1 s and 2p in Paschen notation) excited levels,[41] considering the production/loss of both the metastable and resonant populations.[44] The hypothesis of quasi-isotherm plasma used in earlier works[7,36] has been removed, and a general energy transport equation for electrons[45] has been implemented. Finally, the notorious problem of anomalous diffusion[46] has been addressed, modifying the transport parameters according to Boeuf and Garrigues.[43]

Two different numerical setups have been adopted to compare the results provided by the earlier formulation of 3D-VIRTUS and the upgraded version. In Sec. III, a simplified configuration of a HPT has been used to analyze the influence of each aspect (i.e., chemistry, energy equation, and anomalous diffusion) on both the predicted plasma profiles and the estimated propulsive performance.[39] In Sec. IV, measures performed on a Piglet reactor[47] have been used as benchmark to validate the generalized fluid module implemented on 3D-VIRTUS.

II. METHODOLOGY

The 3D-VIRTUS code solves self-consistently the wave propagation and the plasma transport in a helicon source.[7] The wave propagation is handled in a 3D domain,[37] so the antenna can have a generic shape. In this paper, the plasma transport is solved with a 2D-axisymmetric approach, namely, the walls of the source and the magnetic field can have a generic axisymmetric geometry (e.g., magnetic cusps can be handled).[7] Whether the propulsive performance is computed via an analytical model, the shape of the magnetic field shall respect the paraxial approximation in the region of the acceleration stage.[39]

The validity of the model used to solve the transport in the production stage depends on plasma parameters. First, the DD approximation is used to describe the motion of every species.[48] This condition is strictly respected by heavy species (e.g., ions and neutrals) if the pressure is higher than 10 mTorr[49] and by electrons if the pressure is higher than 1 mTorr.[50] Second, ions are assumed to be non-magnetized since, in typical HPTs, the cyclotron radius is large compared to the characteristic scale-length of the discharge.[5,6] Third, the heavy species are assumed isothermal.[49–52] This is partially justified by experimental evidences on helicon sources reporting an ion temperature in the order of hundreds of Kelvin, apart in the lower hybrid frequency range.[53] Finally, according to experimental evidences on helicon sources, assuming a Maxwellian distribution function for the ions is reasonable unless in the lower hybrid frequency range[53] for the electrons for pressures larger than 1 mTorr.[50]

The numerical strategy to couple 3D-VIRTUS and the analytical plume model is depicted in Fig. 2. The fluid and the EM module are iterated up to convergence after having initialized the plasma profiles. Subsequently, the plasma profiles at the thruster outlet are used as input for the plume model that estimates the propulsive performance. Further details on the numerical implementation of each module and the loop can be found in Refs. 7, 36, and 37. Considering the scope of this paper, the simulation strategy depicted in Fig. 2 has been exploited only partially. In Sec. III, the fluid module of 3D-VIRTUS is coupled to the analytical plume solver since the power deposition profile has been assumed. The latter hypothesis is done to focus on the influence that plasma chemistry, energy equation, and anomalous diffusion have on the plasma transport. In Sec. IV, both the fluid and the EM module are run iteratively, but the plume model has not been adopted since numerical results are benchmarked against measures of plasma density.[47]

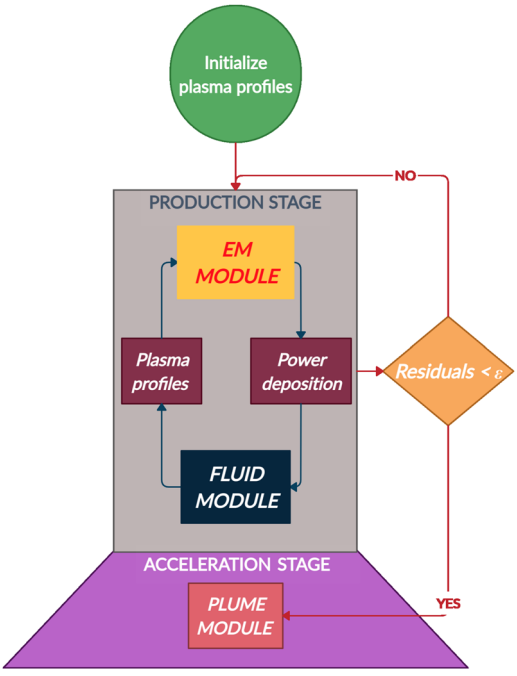

FIG. 2. HPT simulation strategy.

A. Transport equations

The set of governing equations consists in the continuity equation for each species, energy equation for the electrons, and Poisson's equation,

$$\frac{\partial n_k}{\partial t} + \nabla \cdot \boldsymbol{\Gamma}_k = R_k, \tag{1a}$$

$$\frac{\partial}{\partial t}\left(\frac{3}{2} q n_e T_e\right) + \nabla \cdot \left(\frac{5}{2} q T_e \boldsymbol{\Gamma}_e + \overline{\overline{k}}_e \nabla T_e\right) + q\boldsymbol{E} \cdot \boldsymbol{\Gamma}_e = R_\varepsilon + P_\varepsilon, \tag{1b}$$

$$\varepsilon_0 \nabla^2 \phi = -q(n_i - n_e), \tag{1c}$$

where n_k is the density of the kth species (i.e., electrons, ions, neutrals, and excited), T_e is the electron temperature (in eV), ϕ is the electrostatic potential, q is the elementary charge, ε_0 is the vacuum permittivity, and $\boldsymbol{E} = -\nabla\phi$ is the electrostatic field arising from charge unbalance. According to the DD approximation of the momentum equation,[42,54] the particles fluxes read

$$\boldsymbol{\Gamma}_k = \pm \overline{\overline{\mu}}_k n_k \boldsymbol{E} - \overline{\overline{D}}_k n_k \frac{\nabla p_k}{p_k} + n_k \boldsymbol{u_0}, \tag{2}$$

where p_k is the pressure of the kth species, $\boldsymbol{u_0}$ is the convection speed,[7] and $\overline{\overline{\mu}}_k$ and $\overline{\overline{D}}_k$ are the transport coefficients, namely, the mobility (which is null for neutral particles) and the diffusivity, respectively. The expression of the transport coefficients for non-magnetized species (i.e., ions and neutrals) is a diagonal tensor,[36] instead for electrons,

$$\overline{\overline{\mu_e}} = \mu_e \overline{\overline{T_r}}, \quad \overline{\overline{D_e}} = D_e \overline{\overline{T_r}}, \tag{3}$$

where $\mu_e = q/m_e \nu_c$ is the isotropic mobility, m_e is the electron mass, and ν_c is the collision frequency.[41] The isotropic diffusivity is given by the Einstein relation $D_k = \mu_k T_k$ (with T_k in eV).[36] $\overline{\overline{T_r}}$ is the transport tensor, which is defined—when the anomalous transport is not considered (see Sec. II C)—as[55]

$$\overline{\overline{T_r}} = \frac{1}{1+|\chi_c|^2}\begin{pmatrix} 1+\chi_x^2 & \chi_x\chi_y - \chi_z & \chi_x\chi_z + \chi_y \\ \chi_x\chi_y + \chi_z & 1+\chi_y^2 & \chi_y\chi_z - \chi_x \\ \chi_x\chi_z - \chi_y & \chi_y\chi_z + \chi_x & 1+\chi_z^2 \end{pmatrix}, \tag{4}$$

where $\boldsymbol{\chi}_c = (\chi_x, \chi_y, \chi_z)$ is the Hall parameter expressed in terms of the intensity of the magnetic field along the axes (x, y, z), respectively.[55] The sink/source terms (R_k and R_ε) come from the plasma

chemistry.[41] P_ε is the RF power deposited by the antenna, and whether calculated by the EM module of 3D-VIRTUS,[37] it reads

$$\varepsilon_{\text{power}} = \frac{1}{2}\text{Re}\{\boldsymbol{J}_P^\star \cdot \boldsymbol{E}_P\}, \tag{5}$$

where $\boldsymbol{J}_P$ and $\boldsymbol{E}_P$ are the polarization current and the local value of electric field inside the plasma, respectively. Finally, it is worth noting that the electron energy equation [Eq. (1b)] does not rely on the quasi-isotherm hypothesis enforced in previous works.[7,8,36] Specifically, the thermal diffusivity reads $\overline{\overline{k_e}} = 5/2 n_e \overline{\overline{D_e}}$.[32,42,45]

Boundary conditions are prescribed as in Ref. 7. In each boundary of the domain, a Robin condition is assumed for the continuity and the energy of the electrons in order to enforce the Bohm sheath criterion;[42] this implies that the thruster outlet is sonic.[39] The Neumann condition that applies to the ion continuity is also determined according to the Bohm sheath criterion.[7] A Dirichlet condition applies to every boundary of the domain for the solution of the Poisson's equation, in particular, the thruster outlet is assumed at the ground.[9] At the walls of the source, excited species diffuse according to the thermal motion, while the neutral flux is determined by the recombination of ionized and excited species.[42] At the thruster inlet/outlet, the motion of the excited and the neutral species is solely due to convection.[7] Further details on the Neumann/Robin boundary conditions that apply to the continuity of excited and neutral species are reported in Ref. 7.

B. Plasma chemistry

A collisional-radiative model (CRM) was built in order to reproduce the dynamics of an argon plasma when the excited levels are considered.[41] Specifically, the 1s and 2p excited levels (shown in Table I) along with the ground state and the first ionized level have been simulated. Taking into account only 1s and 2p excited species is justified since the working pressure of typical HPTs is sufficiently low (i.e., tenths of mTorr or lower) that the density of higher excitation levels is negligible according to experiments.[56] The excited species reported in Table I have been lumped into three equivalent states, namely, 1s metastable ($1s_M$), 1s resonant ($1s_R$), and 2p (see Table II) in order to reduce the number of fluid equations.[41] The reactions considered are reported in Table III and schematically depicted in Fig. 3. The procedure to calculate the reaction rates, the diffusion coefficients, and with the source/sink terms in Eqs. (1a) and (1b) in case of a Maxwellian electron distribution function has been thoroughly discussed in Refs. 41 and 57.

TABLE I. Argon excited levels in Paschen notation.[44]

Level	Excitation energy (eV)
GS	0
$1s_5$	11.548
$1s_4$	11.623
$1s_3$	11.723
$1s_2$	11.828
$2p_{10}$	12.907
$2p_9$	13.076
$2p_8$	13.095
$2p_7$	13.153
$2p_6$	13.172
$2p_5$	13.273
$2p_4$	13.283
$2p_3$	13.302
$2p_2$	13.328
$2p_1$	13.480
ION	15.76

TABLE II. Ar species considered in the CRM.

Species	
Ar_{GS}	Ground state
Ar_{1sM}	$1s_5$, $1s_3$ (metastable)
Ar_{1sR}	$1s_4$, $1s_2$ (resonant)
Ar_{2p}	$2p_{10}$, $2p_9$, $2p_8$, $2p_7$, $2p_6$, $2p_5$, $2p_4$, $2p_3$, $2p_2$, $2p_1$
Ar^+	First ionized argon
e	Electron

C. Anomalous diffusion

The anomalous transport is an empirically observed discrepancy between the values of the diffusion coefficients computed classically (see Sec. II A) and the ones measured in experiments. This phenomenon can be attributed to the establishment of turbulence, which is broken down by instabilities of the magnetic field.[58] The classical definition of the electron diffusion coefficient across a magnetic field reads[59]

$$D_\perp = \frac{qT_e\nu_c}{m_e\omega_B{}^2} \sim \frac{1}{B^2}, \tag{6}$$

TABLE III. Reactions considered in the CRM.

$Ar_{GS} + e \rightleftharpoons Ar_{1sM} + e$	Excitation
$Ar_{GS} + e \rightleftharpoons Ar_{1sR} + e$	Excitation
$Ar_{GS} + e \rightleftharpoons Ar_{2p} + e$	Excitation
$Ar_{1sM} + e \rightleftharpoons Ar_{1sR} + e$	Excitation
$Ar_{1sM} + e \rightleftharpoons Ar_{2p} + e$	Excitation
$Ar_{1sR} + e \rightleftharpoons Ar_{2p} + e$	Excitation
$Ar_{GS} + e \rightleftharpoons Ar_{GS} + e$	Elastic scattering
$Ar_{1sM} + e \rightleftharpoons Ar_{1sM} + e$	Elastic scattering
$Ar_{1sR} + e \rightleftharpoons Ar_{1sR} + e$	Elastic scattering
$Ar_{2p} + e \rightleftharpoons Ar_{2p} + e$	Elastic scattering
$Ar_{GS} + e \rightarrow Ar_+ + 2e$	Ionization
$Ar_{1sM} + e \rightarrow Ar_+ + 2e$	Ionization
$Ar_{1sR} + e \rightarrow Ar_+ + 2e$	Ionization
$Ar_{2p} + e \rightarrow Ar_+ + 2e$	Ionization
$Ar_{1sR} \rightarrow Ar_{GS} + h\nu$	Radiative decay
$Ar_{2p} \rightarrow Ar_{1sM} + h\nu$	Radiative decay
$Ar_{2p} \rightarrow Ar_{1sR} + h\nu$	Radiative decay

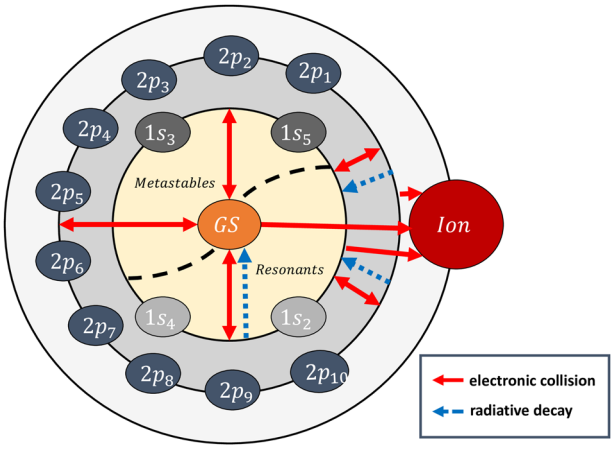

FIG. 3. Schematic of the reactions considered in the CRM.[41]

where ω_B is the cyclotron frequency.[59] Bohm found that the upper limit of the diffusion coefficient behaves rather like[46]

$$D_{Bohm} = \frac{1}{16}\frac{T_e}{B} \sim \frac{1}{B}. \tag{7}$$

In order to account for this phenomenon, Boeuf and Garrigues[43] suggested to modify the collisional frequency in the momentum equation adding a term proportional to the cyclotron frequency,

$$\nu_{\text{Bohm}} = \nu + \alpha\omega_C, \tag{8}$$

where α is an empirical coefficient that should be adjusted to match experiments. Assuming an axially oriented magnetic field $\boldsymbol{B_0} = (0, 0, B_z)$, this methodology leads to the following formulation of the transport matrix:

$$\overline{\overline{T_r}} = \frac{1}{{\chi_z}^2 + (1+\alpha\chi_z)^2}\begin{pmatrix} 1+\alpha\chi_z & -\chi_z & 0 \\ \chi_z & 1+\alpha\chi_z & 0 \\ 0 & 0 & {\chi_z}^2 + (1+\alpha\chi_z)^2 \end{pmatrix}. \tag{9}$$

In case of a generically oriented magnetic field, the transport matrix is obtained via the tensor rotation approach suggested by Sanchez-Villar *et al.*[32]

III. NUMERICAL ANALYSIS

The scope of this section is to quantify the influence that different formulations of the plasma chemistry, the energy equation, and the diffusion model have on the numerical results. To this end, a simplified geometry representative of a medium-low power HPT[3] has been adopted [see Fig. 4(a)]. The helicon source has a cylindrical shape of length $L = 0.10$ m and radius $R = 0.05$ m. The magnetic field is generated by Helmholtz coils, as in the prototype proposed by Ziemba *et al.*[60] Inside the source, the magnetic field is quasi-axial and the intensity at the thruster outlet is $B_0 = 500$ G.[20] The parameters analyzed in the following are the electron density (n_e) and temperature (T_e) profiles computed from the fluid module of 3D-VIRTUS along with the thrust (T) and the specific impulse (I_{sp}) provided by the analytical plume model.[39] The power deposition profile has been

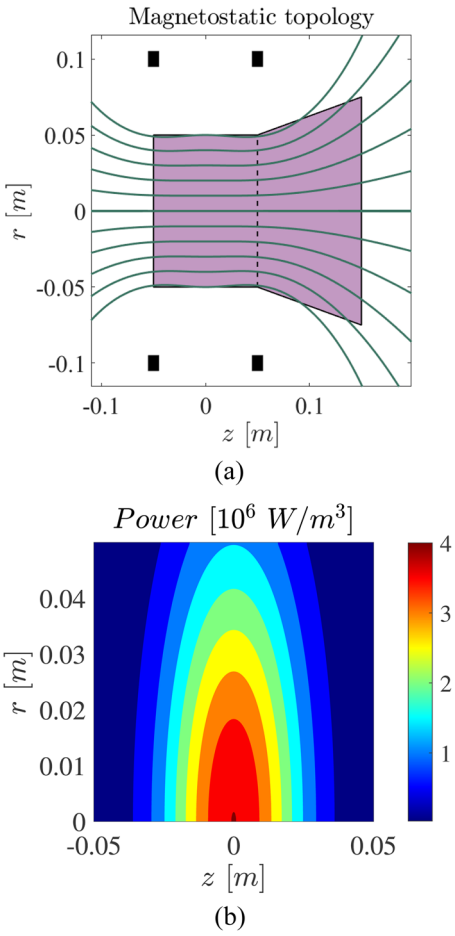

FIG. 4. (a) Schematic of the simplified HPT considered for the numerical analysis; magnetic field lines and Helmholtz coils have been highlighted. (b) Assumed power deposition profile.

assumed and not computed [see Fig. 4(b)] in order to (i) focus on the effect that each phenomenon (i.e., plasma chemistry, energy equation, and anomalous diffusion) has on the fluid model, neglecting the indirect influence of the power deposition profile, (ii) understanding whether these phenomena have a major role in the determination of the propulsive performance. The total power coupled to the plasma is $Pw = 12$ W. The system is fed with argon gas at initial temperature $T_0 = 300$ K. The propellant mass-flow rate ($\dot{m}_0$) has

TABLE IV. Parameters used in the simulations of the simplified HPT.

Parameters of the simulations	
R	0.05 m
L	0.10 m
B_0	500 G
Pw	12 W
T_0	300 K
$\dot{m}_0$	0.5–50 mg/s
n_0	10^{19}–10^{21} m^{-3}

been varied in the range from 0.5 to 50 mg/s so that the operational neutral density (n_0) is in the range from 10^{19}–10^{21} m^{-3}. Referring to Fig. 4(a), the surface at $z = -0.05$ m is considered the thruster inlet, while the surface at $z = 0.05$ m is the outlet (boundary conditions are defined coherently). In the rest of this section, the convection speed is assumed aligned along the axis of the thruster and its magnitude is $u_0 = 1/4v^{th}$, where v^{th} is the thermal speed of neutral species.[7] Reaction rates that govern the plasma chemistry are assumed according to Zhu and Pu.[61] The discretization of the computational domain consisted of a structured mesh of 31 250 hexahedra. The temporal discretization is done via an explicit Euler scheme with an integration time step of 10^{-8} s. In Table IV, the parameters used in the simulations of the simplified HPT are shown.

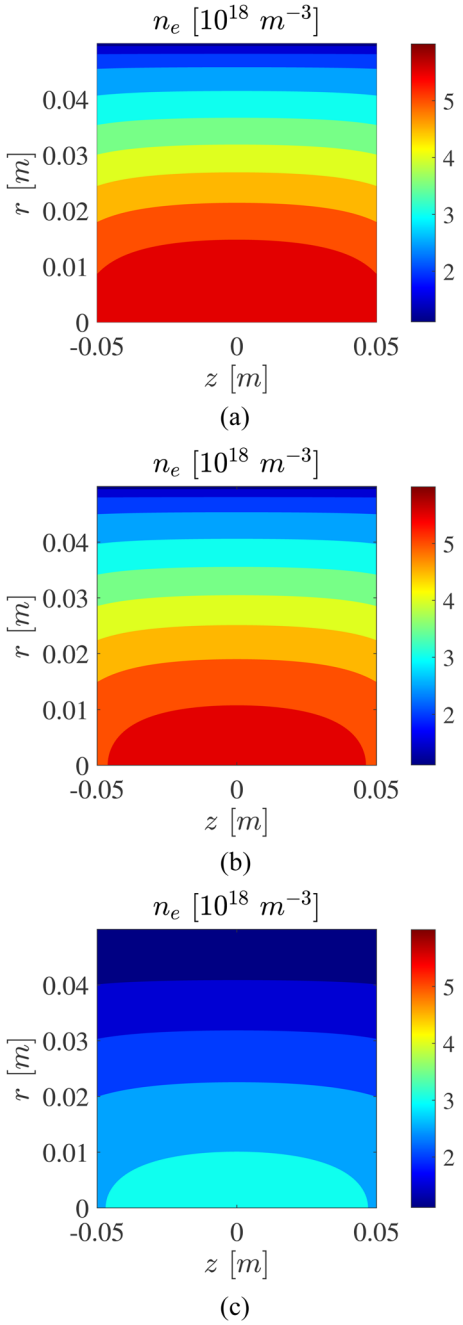

FIG. 5. Electron density (n_e) within the helicon source as a function of the radial (r) and axial (z) coordinates. (a) OLD chemical model, (b) CM, and (c) CRM.

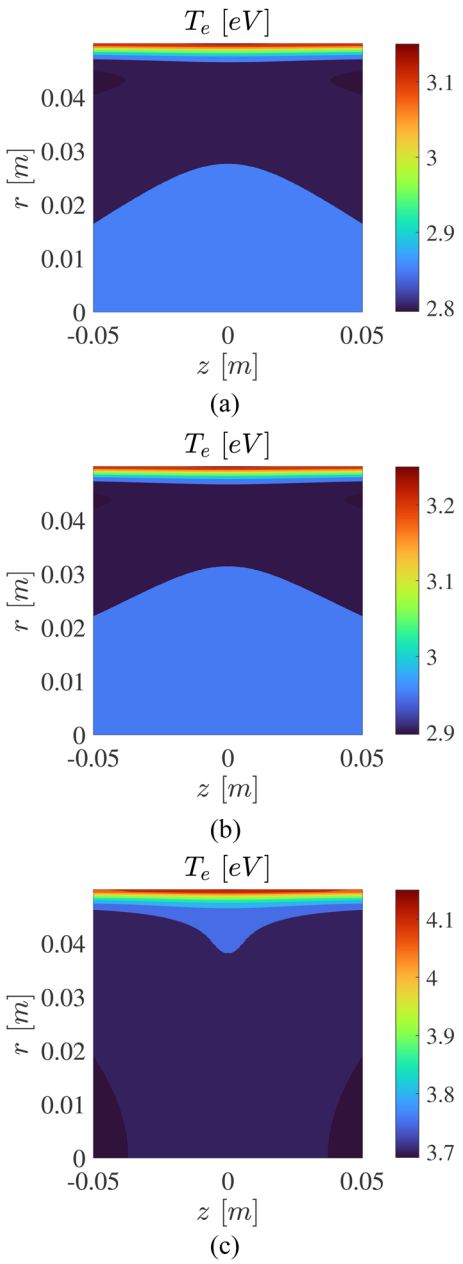

FIG. 6. Electron temperature (T_e) within the helicon source as a function of the radial (r) and axial (z) coordinates. (a) OLD chemical model, (b) CM, and (c) CRM.

TABLE V. Propulsive performance obtained using three different plasma chemistry models.

Model	T (mN)	I_{sp} (s)
OLD	59.6	1101
CM	59.9	1104
CRM	40.6	741

A. Plasma chemistry

The results obtained with the plasma chemistry model proposed in Magarotto *et al.*[36] (i.e., excited condensed in only one equivalent species) have been compared against the ones attained with the formulation discussed in Sec. II B. Two versions of the upgraded chemical model have been considered, namely, neglecting or considering radiative decay reactions (see Table III). Hereinafter, the chemistry model proposed by Magarotto *et al.*[36] has been referred to as OLD, the new model in which the radiative decay is neglected as CM (collisional model), and the last one as CRM (collisional-radiative model). The assumed mass flow rate is $\dot{m}_0 = 5$ mg/s, namely, the operational neutral density is $n_0 \approx 10^{20}$ m^{-3}, the quasi-isotherm formulation of the energy equation is adopted,[36] and the anomalous transport has been neglected.

Plasma density and electron temperature profiles obtained with the three formulations of the plasma chemistry are depicted in Figs. 5 and 6, respectively. There are not significant differences (lower than 5%) between OLD and CM both in terms of electron density and temperature. On the other hand, the electron density computed with CRM is almost 60% lower with respect to CM and OLD; the temperature peak is 25% higher. This is due to the loss mechanisms associated with the decay of the excited states toward lower energy levels.[41] In Table V, the propulsive performance is reported, and a drop of about 40% can be seen comparing CRM and CM/OLD.

B. Energy equation

In Ref. 36, the energy equation was determined according to the quasi-isotherm hypothesis. In this work, a more general formulation is proposed in which the contribution of the heat flux is taken into account [see Eq. (1b)]. In the following, the plasma chemistry is handled according to *CM*, the anomalous transport is not considered, and the mass flow rate is $\dot{m}_0 = 5$ mg/s ($n_0 \approx 10^{20}$ m^{-3}).

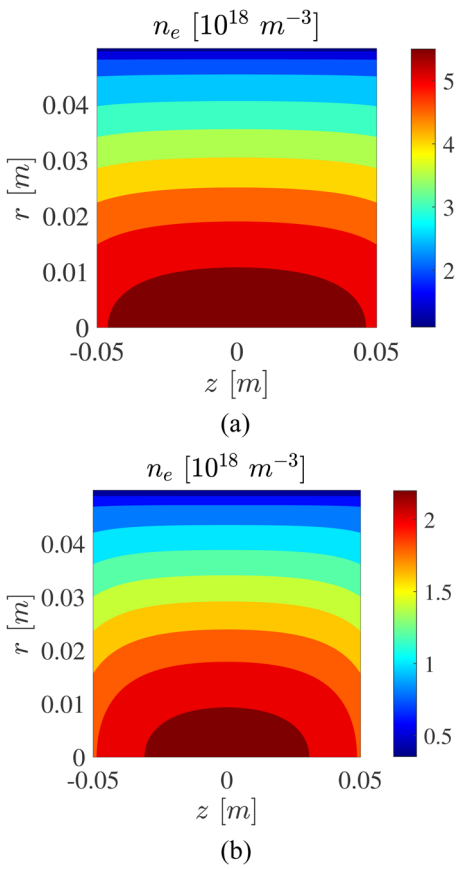

FIG. 7. Electron density (n_e) within the helicon source as a function of the radial (r) and axial (z) coordinates. (a) Q-I and (b) FE formulations of the energy equation.

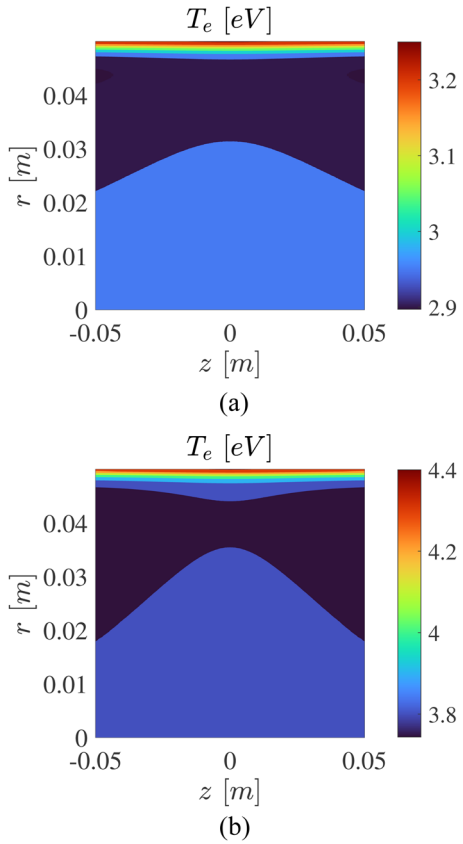

FIG. 8. Electron temperature (T_e) within the helicon source as a function of the radial (r) and axial (z) coordinates. (a) Q-I and (b) FE formulations of the energy equation.

In Figs. 7 and 8, the electron density and temperature obtained enforcing the quasi-isotherm hypothesis (referred to as Q-I) or solving the full energy equation (referred to as FE) are reported. There are non-negligible differences between the two formulations. Considering FE, n_e decreases of almost 33% with respect to Q-I and T_e increases of more than 1 eV. This result is associated with a higher energy loss predicted from FE with respect to Q-I with the assumed geometric/magnetic configuration.

C. Anomalous diffusion

The effects of the anomalous diffusion have been analyzed via a sensitivity analysis over the parameter α [see Eq. (8)]. The Q-I hypothesis and the CM formulation are assumed along with three different values of the mass flow rate are considered, namely, $\dot{m}_0$ = 0.5, 5, and 50 mg/s ($n_0 \approx 10^{19}$, 10^{20}, and 10^{21} m^{-3}).

In Fig. 9, the results are depicted in terms of peak electron density and temperature, while in Fig. 10, thrust and specific impulse are reported. The magnitude of α affects plasma density up to 50% with minimum in correspondence of $\alpha \approx 1$ and maximum for $\alpha = 0$. Limiting the analysis to $\alpha \leq \alpha_{Bohm} = 1/16$, n_e varies no more than 10% in terms of α (the higher the $\dot{m}_0$, the lower the influence of α on n_e). T_e is instead affected less than ±0.5 eV by α. This can be explained with a general lower magnetic confinement associated with the anomalous diffusion with respect to the classical formulation.[58] Consequently, the choice of α influences less than 20% the estimation of thrust and specific impulse.

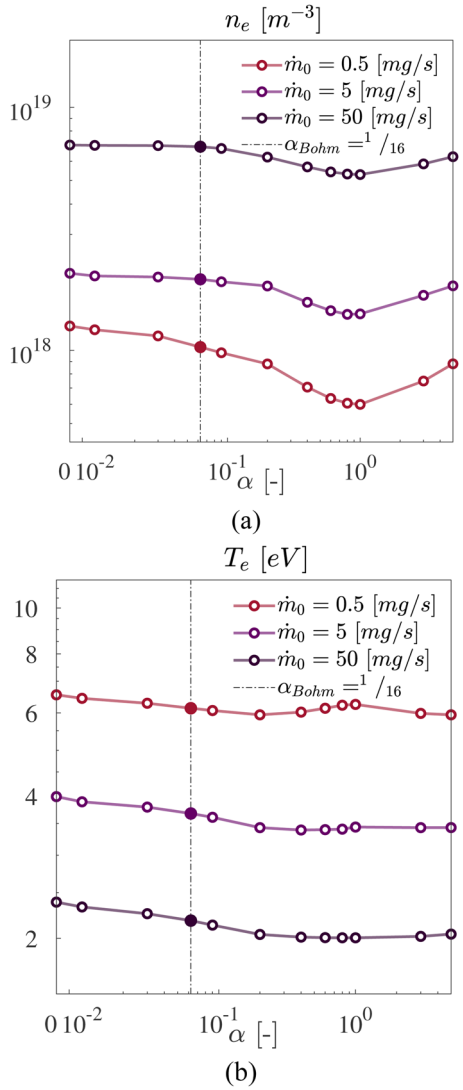

FIG. 9. (a) Peak electron density n_e and (b) peak electron temperature T_e as a function of the anomalous diffusion parameter α. Three values of the mass flow rate $\dot{m}_0$. The dashed line indicates α_{Bohm} = 1/16.

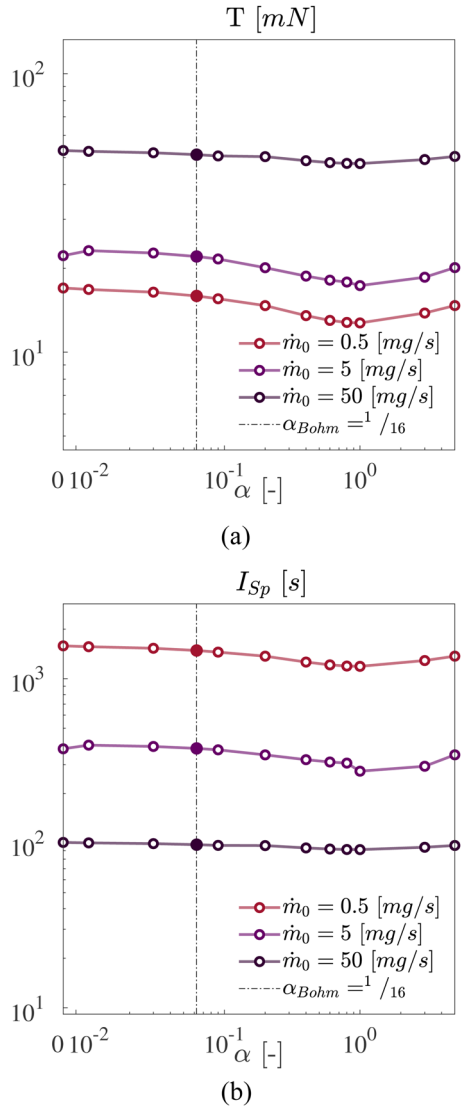

FIG. 10. (a) Thrust T and (b) specific impulse I_{sp} as a function of the anomalous diffusion parameter α. Three values of the mass flow rate $\dot{m}_0$. The dashed line indicates α_{Bohm} = 1/16.

IV. EXPERIMENTAL VALIDATION

The upgrades of the code discussed in Secs. II and III have been benchmarked against experimental data collected on a helicon source, namely, the Piglet reactor analyzed in the work of Lafleur *et al.*[47] The setup is composed of a discharge camber (i.e., a dielectric tube) in which the plasma is produced and heated up,[36] along with an expansion chamber. The discharge chamber is 0.2 m long with a diameter of 0.136 m and is driven by a double-saddle antenna wrapped around the dielectric tube. The antenna powered at 250 W and at a frequency of 13.56 MHz generates the plasma within the discharge chamber. A 500 turn electromagnetic coil is positioned near the source exit and generates a magnetic field of intensity up to 2.1 mT. The source is filled with argon through a port in the diffusion chamber, and the gas pressure is 2.7 mTorr. For further details on the experimental setup, see Ref. 47. The electron density has been measured along the axis of the discharge with a Langmuir probe operated in ion saturation mode.

In Table VI, the input parameters considered for the numerical simulation are reported. The generalized formulation of the energy equation is assumed, the chemistry model discussed in Sec. II B has been adopted, and $\alpha = 0$. The power deposition profile is calculated with the EM module of 3D-VIRTUS, and not assumed, in order to be more adherent with reality. The plasma transport is handled with the fluid module, and the whole simulation is carried out through the iterative convergence cycle described in Sec. II. Regarding the chemistry data considered for the simulations, the reaction rates coefficients reported in Souhair *et al.*[41] have been adopted. All the boundaries of the simulation domain have been treated as walls (see Sec. II A); therefore, the analytical plume model has not been used. Moreover, the validation is focused on the upgrades of the fluid model, namely, the simulation of the discharge chamber is paramount with respect to the expansion of the plasma. The fluid domain consists of a 2D-axisymmetric structured hexa-mesh of 11 000 elements. For what the EM domain is concerned, the source is made of an unstructured mesh of about 10 000 tetrahedral elements.

The electron density profile along the axis of the Piglet reactor has been calculated and benchmarked against measures. The results obtained and the reference experimental data are depicted in Fig. 11. Measures performed with the Langmuir probe are affected by an uncertainty of ±25%.[36] A confidence interval (referred to as numerical envelope) has been associated with the results of the simulations. The first source of numerical uncertainty is due to cross sections. The variance associated with the choice of this parameter from different authors is delimited by the *Upper* and the *Lower* cases in Fig. 11 (for further details, refer to Ref. 41). Moreover, an additional

TABLE VI. Input parameters used to simulate the Piglet reactor.

Parameter	Value
Source diameter	0.136 m
Source length	0.2 m
RF power	250 W
Antenna frequency	13.56 MHz
Magneto-static field (peak)	2.1 mT
Gas pressure	2.7 mTorr

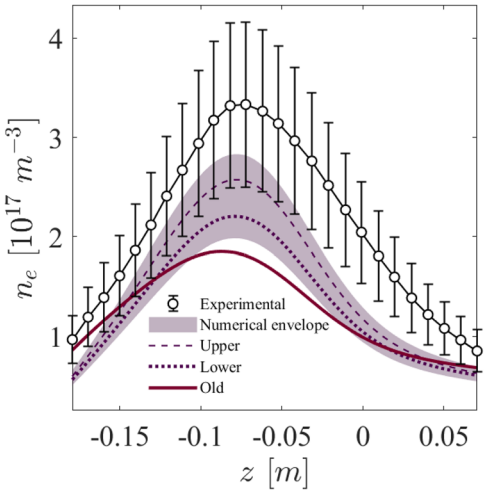

FIG. 11. Electron density n_e as a function of the axial position z. Experimental data have been formerly presented in Ref. 47. The extremes of the numerical envelope determined by the choice of the cross section are labeled *Upper* and *Lower*. Data provided with the formulation proposed in Ref. 36 are labeled *Old*.

10% of uncertainty above and below these two extremes is related to further approximations on the input parameters of the model. One of the main sources of uncertainties is the DD hypothesis, which becomes less robust when dealing with low pressure discharges (i.e., few mTorr).[36] In addition, the assumption of Maxwellian distribution function for the electrons may not always be accurate, e.g., this is particularly true in proximity of the walls where the sheath forms[62] and in the expansion chamber where a bi-Maxwellian might occur.[36] Other sources of uncertainty are related to the isotherm hypothesis for the heavy species and to the assumption of non-magnetized ions that might affect the results as well. However, each of these errors is expected to be in the order of few percent points.[36] The results obtained with the formulation of the fluid module proposed in Magarotto *et al.*[36] have been reported as well in Fig. 11 (labeled *Old*).

The numerical envelope follows remarkably well the trend of the measured electron density, although the results underestimate the experimental data. Nonetheless, numerical predictions overlap the uncertainty band of the measures, thus providing an overall satisfactory agreement with the reference experimental data. The disagreement between numerical results and measures in terms of peak plasma density is in the order of 20% and 40% for the *Upper* and *Lower* cases, respectively. Specifically, the improvement with respect to the *Old* model is particularly evident, since the value of the plasma density peak increases 15%–30% with the new formulation of the fluid module.

V. CONCLUSIONS

In this work, the plasma transport within the helicon source of a HPT has been analyzed. Results provided with different formulations of the plasma chemistry model, the electron energy equation, and the diffusion coefficients have been quantitatively compared relying on the numerical tool 3D-VIRTUS.[36]

The effect produced by each single aspect on the electron density and temperature profiles, along with the thrust and the specific impulse in case of a medium-low power HPT,[3] has been assessed. To this end, a simplified helicon source for space application has been studied, plasma profiles are computed with the fluid module of 3D-VIRTUS,[36] and the propulsive performance is estimated with the analytical model proposed by Lafleur.[39] Lumping different excitation levels in one or three equivalent species has a minor effect on the results of the simulation (n_e and T_e affected for less than 5%). On the contrary, the energy losses due to radiative decay reactions affect the propulsive performance up to 40%. Formulating the electron energy equation with the quasi-isotherm hypothesis or accounting for the heat flux results in estimations of the electron density that differ for about 30%. Defining the diffusion coefficients according to the classical formulation or the anomalous transport does not have a major influence on the propulsive performance (<20%).

Moreover, the results provided by the generalized formulation of the fluid module have been benchmarked against measures of the electron density performed on a Piglet reactor.[47] To this end, both the plasma transport and the power deposition profiles are solved with 3D-VIRTUS and simulations are carried out through an iterative convergence cycle.[36] The experimental trend is reproduced by numerical results, and the disagreement on the plasma density peak is lower than 20%, namely, within the uncertainty band of the measures. With respect to the formulation of the fluid module proposed by Magarotto *et al.*,[36] the quantitative agreement between simulations and experiments increases about 30%.

In future works, the development, implementation, and validation[63] of a fully coupled set of continuity, momentum, and energy equations will be presented, dropping the DD hypothesis for heavy species. In this way, it will be possible to simulate both the production and the acceleration stages of a HPT with a single self-consistent numerical tool. This work is currently on-going at the University of Bologna[24] and the University of Padova. Finally, it is worth mentioning that self-consistent numerical tools capable of simulating the plasma dynamics in RF sources are of interest not only for space applications but also in the fields of material processing[46] and lightning,[64] along with radar and telecommunications.[65–69]

ACKNOWLEDGMENTS

We acknowledge Technology for Propulsion and Innovation S.p.A. for the support provided in the development of this work.

AUTHOR DECLARATIONS

Conflict of Interest

The authors have no conflicts to disclose.

DATA AVAILABILITY

The data that support the findings of this study are available from the corresponding author upon reasonable request.

REFERENCES

[1] R. G. Jahn, *Physics of Electric Propulsion* (Courier Corporation, 2006).
[2] G. P. Sutton and O. Biblarz, *Rocket Propulsion Elements* (John Wiley & Sons, 2016).
[3] K. Takahashi, "Helicon-type radiofrequency plasma thrusters and magnetic plasma nozzles," Rev. Mod. Plasma Phys. **3**, 3 (2019).
[4] F. F. Chen, "Helicon discharges and sources: A review," Plasma Sources Sci. Technol. **24**, 014001 (2015).
[5] M. Manente, F. Trezzolani, M. Magarotto, E. Fantino, A. Selmo, N. Bellomo, E. Toson, and D. Pavarin, "REGULUS: A propulsion platform to boost small satellite missions," Acta Astronaut. **157**, 241–249 (2019).
[6] N. Bellomo, M. Magarotto, M. Manente, F. Trezzolani, R. Mantellato, L. Cappellini, D. Paulon, A. Selmo, D. Scalzi, M. Minute *et al.*, "Design and in-orbit demonstration of regulus, an iodine electric propulsion system," CEAS Space J. (to be published) (2021).
[7] M. Magarotto, M. Manente, F. Trezzolani, and D. Pavarin, "Numerical model of a helicon plasma thruster," IEEE Trans. Plasma Sci. **48**, 835–844 (2020).
[8] M. Magarotto and D. Pavarin, "Parametric study of a cathode-less radio frequency thruster," IEEE Trans. Plasma Sci. **48**, 2723–2735 (2020).
[9] E. Ahedo and M. Merino, "Two-dimensional supersonic plasma acceleration in a magnetic nozzle," Phys. Plasmas **17**, 073501 (2010).
[10] J. Zhou, G. Sánchez-Arriaga, and E. Ahedo, "Time-dependent expansion of a weakly-collisional plasma beam in a paraxial magnetic nozzle," Plasma Sources Sci. Technol. **30**, 045009 (2021).
[11] D. M. Goebel and I. Katz, *Fundamentals of Electric Propulsion: Ion and Hall Thrusters* (John Wiley & Sons, Inc., 2008), pp. 1–507.
[12] F. Romano, Y.-A. Chan, G. Herdrich, C. Traub, S. Fasoulas, P. C. E. Roberts, K. Smith, S. Edmondson, S. Haigh, N. H. Crisp *et al.*, "RF helicon-based inductive plasma thruster (IPT) design for an atmosphere-breathing electric propulsion system (ABEP)," Acta Astronaut. **176**, 476–483 (2020).
[13] A. E. Vinci and S. Mazouffre, "Direct experimental comparison of krypton and xenon discharge properties in the magnetic nozzle of a helicon plasma source," Phys. Plasmas **28**, 033504 (2021).
[14] M. D. West, C. Charles, and R. W. Boswell, "Testing a helicon double layer thruster immersed in a space-simulation chamber," J. Propul. Power **24**, 134–141 (2008).
[15] D. Pavarin, F. Ferri, M. Manente, D. Rondini, D. Curreli, Y. Guclu, M. Melazzi, S. Suman, and G. Bianchini, "Helicon plasma hydrazine combined micro project overview and development status," in Proceedings of the 2nd Space Propulsion Conference SP2010-1842379, San Sebastian, 2010.
[16] F. Trezzolani, M. Manente, A. Selmo, D. Melazzi, M. Magarotto, D. Moretto, P. D. Carlo, M. Pessana, and D. Pavarin, "Development and test of an high power RF plasma thruster in project sapere-strong," in The 35th International Electric Propulsion Conference IEPC-2017-462, Atlanta, GA, 2017.
[17] See https://www.t4innovation.com/it/ for Technology for propulsion and innovation.
[18] F. R. C. Díaz, "The Vasimr rocket," Sci. Am. **283**, 90–97 (2000).
[19] M. Ruiz, V. Gomez, P. Fajardo, J. Navarro, R. Albertoni, G. Dickeli, A. Vinci, S. Mazouffre, and N. Hildebrand, "HIPATIA: A project for the development of the helicon plasma thruster and its associated technologies to intermediate-high TRLs," in 71st International Astronautical Congress (IAC), Washington, DC, 2020.
[20] K. Takahashi, "Magnetic nozzle radiofrequency plasma thruster approaching twenty percent thruster efficiency," Sci. Rep. **11**, 2768 (2021).
[21] O. V. Batishchev, "Minihelicon plasma thruster," IEEE Trans. Plasma Sci. **37**, 1563–1571 (2009).
[22] J. Sheehan, T. A. Collard, F. H. Ebersohn, and B. W. Longmier, "Initial operation of the cubesat ambipolar thruster," in 34th International Electric Propulsion Conference, IEPC-2015-243, Hyogo-Kobe, 2015.
[23] R. Winglee, T. Ziemba, L. Giersch, J. Prager, J. Carscadden, and B. R. Roberson, "Simulation and laboratory validation of magnetic nozzle effects for the high power helicon thruster," Phys. Plasmas **14**, 063501 (2007).
[24] See https://site.unibo.it/apl/ for Alma propulsion laboratory.
[25] D. Bose, T. R. Govindan, and M. Meyyappan, "Modeling of a helicon plasma source," IEEE Trans. Plasma Sci. **31**, 464–470 (2003).
[26] M. Martinez-Sanchez, J. Navarro-Cavallé, and E. Ahedo, "Electron cooling and finite potential drop in a magnetized plasma expansion," Phys. Plasmas **22**, 053501 (2015).

[27]E. Ahedo, S. Correyero, J. Navarro-Cavallé, and M. Merino, "Macroscopic and parametric study of a kinetic plasma expansion in a paraxial magnetic nozzle," Plasma Sources Sci. Technol. **29**, 045017 (2020).
[28]Y. Takao and K. Takahashi, "Numerical validation of axial plasma momentum lost to a lateral wall induced by neutral depletion," Phys. Plasmas **22**, 113509 (2015).
[29]G. Gallina, M. Magarotto, M. Manente, and D. Pavarin, "Enhanced bidimensional pic: An electrostatic/magnetostatic particle-in-cell code for plasma based systems," J. Plasma Phys. **85**, 905850205 (2019).
[30]F. Cichocki, A. Domínguez-Vázquez, M. Merino, and E. Ahedo, "Hybrid 3D model for the interaction of plasma thruster plumes with nearby objects," Plasma Sources Sci. Technol. **26**, 125008 (2017).
[31]J. Zhou, D. Pérez-Grande, P. Fajardo, and E. Ahedo, "Numerical treatment of a magnetized electron fluid model within an electromagnetic plasma thruster simulation code," Plasma Sources Sci. Technol. **28**, 115004 (2019).
[32]Á. Sánchez-Villar, J. Zhou, E. Ahedo, and M. Merino, "Coupled plasma transport and electromagnetic wave simulation of an ECR thruster," Plasma Sources Sci. Technol. **30**, 045005 (2021).
[33]A. R. Choudhuri, *The Physics of Fluids and Plasmas* (Cambridge University Press, 1998).
[34]J. van Dijk, G. M. W. Kroesen, and A. Bogaerts, "Plasma modelling and numerical simulation," J. Phys. D: Appl. Phys. **42**, 190301 (2009).
[35]G. Chen, "A self-consistent model of helicon discharge," Ph.D thesis, University of Texas at Austin, 2008.
[36]M. Magarotto, D. Melazzi, and D. Pavarin, "3D-virtus: Equilibrium condition solver of radio-frequency magnetized plasma discharges for space applications," Comput. Phys. Commun. **247**, 106953 (2020).
[37]D. Melazzi and V. Lancellotti, "Adamant: A surface and volume integral-equation solver for the analysis and design of helicon plasma sources," Comput. Phys. Commun. **185**, 1914–1925 (2014).
[38]See https://openfoam.org/ for the openfoam foundation.
[39]T. Lafleur, "Helicon plasma thruster discharge model," Phys. Plasmas **21**, 043507 (2014).
[40]S. D. Fede, M. Magarotto, S. Andrews, M. Manente, and D. Pavarin, "Numerical simulation of the plume of a magnetically enhanced plasma thruster," in Proceedings Of the 7th Space Propulsion Conference SP2020-00111, On-line conference, 2020.
[41]N. Souhair, M. Magarotto, E. Majorana, F. Ponti, and D. Pavarin, "Development of a lumping methodology for the analysis of the excited states in plasma discharges operated with argon, neon, krypton, and xenon," Phys. Plasmas **28**, 093504 (2021).
[42]J. D. Bukowski, D. B. Graves, and P. Vitello, "Two-dimensional fluid model of an inductively coupled plasma with comparison to experimental spatial profiles," J. Appl. Phys. **80**, 2614–2623 (1996).
[43]J. P. Boeuf and L. Garrigues, "Low frequency oscillations in a stationary plasma thruster," J. Appl. Phys. **84**, 3541–3554 (1998).
[44]See https://www.nist.gov/pml/atomic-spectra-database for the National Institutes of Standards and Technology—Atomic spectra database; accessed on 1 January 2021.
[45]J. A. Bittencourt, *Fundamentals of Plasma Physics* (Springer, New York, 2004).
[46]M. A. Lieberman and A. J. Lichtenberg, *Principles of Plasma Discharges and Materials Processing*, 2nd ed. (Wiley, 2005).
[47]T. Lafleur, C. Charles, and R. W. Boswell, "Characterization of a helicon plasma source in low diverging magnetic fields," J. Phys. D: Appl. Phys. **44**, 055202 (2011).
[48]A. Fiala, L. C. Pitchford, and J. P. Boeuf, "Two-dimensional, hybrid model of low-pressure glow discharges," Phys. Rev. E **49**, 5607–5622 (1994).
[49]D. Bose, T. R. Govindan, and M. Meyyappan, "Modelling of magnetic field profile effects in a helicon source," Plasma Sources Sci. Technol. **13**, 553–561 (2004).
[50]G. Chen and L. L. Raja, "Fluid modeling of electron heating in low-pressure, high-frequency capacitively coupled plasma discharges," J. Appl. Phys. **96**, 6073–6081 (2004).
[51]H. C. Kim, F. Iza, S. S. Yang, M. Radmilović-Radjenović, and J. K. Lee, "Particle and fluid simulations of low-temperature plasma discharges: Benchmarks and kinetic effects," J. Phys. D: Appl. Phys. **38**, R283–R301 (2005).
[52]S. Rauf, K. Bera, and K. Collins, "Self-consistent simulation of very high frequency capacitively coupled plasmas," Plasma Sources Sci. Technol. **17**, 035003 (2008).
[53]M. M. Balkey, R. Boivin, J. L. Kline, and E. E. Scime, "Ion heating and density production in helicon sources near the lower hybrid frequency," Plasma Sources Sci. Technol. **10**, 284–294 (2001).
[54]M. Abdollahzadeh, J. C. Pascoa, and P. J. Oliveira, "Implementation of the classical plasma–fluid model for simulation of dielectric barrier discharge (DBD) actuators in OpenFOAM," Comput. Fluids **128**, 77–90 (2016).
[55]R. L. Kinder and M. J. Kushner, "Noncollisional heating and electron energy distributions in magnetically enhanced inductively coupled and helicon plasma sources," J. Appl. Phys. **90**, 3699–3712 (2001).
[56]K. E. Evdokimov, M. E. Konischev, V. F. Pichugin, and Z. Sun, "Study of argon ions density and electron temperature and density in magnetron plasma by optical emission spectroscopy and collisional-radiative model," Resour.-Effic. Technol. **3**, 187–193 (2017).
[57]E. Majorana, N. Souhair, F. Ponti, and M. Magarotto, "Development of a plasma chemistry model for helicon plasma thruster analysis," Aerotec., Missili Spazio **1**, 1–14 (2021).
[58]E. Ahedo, J. M. Gallardo, and M. Martínez-Sánchez, "Effects of the radial plasma-wall interaction on the hall thruster discharge," Phys. Plasmas **10**, 3397–3409 (2003).
[59]F. F. Chen, *Introduction to Plasma Physics and Controlled Fusion* (Springer International Publishing, 2016).
[60]T. Ziemba, J. Carscadden, J. Slough, J. Prager, and R. Winglee, "High power helicon thruster," AIAA Paper No. 2005-4119, 2005.
[61]X. M. Zhu and Y. K. Pu, "A simple collisional-radiative model for low-temperature argon discharges with pressure ranging from 1 Pa to atmospheric pressure: Kinetics of Paschen 1s and 2p levels," J. Phys. D: Appl. Phys. **43**, 015204 (2010).
[62]V. V. Gorin, A. A. Kudryavtsev, J. Yao, C. Yuan, and Z. Zhou, "Boundary conditions for drift-diffusion equations in gas-discharge plasmas," Phys. Plasmas **27**, 013505 (2020).
[63]F. Trezzolani, M. Magarotto, M. Manente, and D. Pavarin, "Development of a counterbalanced pendulum thrust stand for electric propulsion," Measurement **122**, 494–501 (2018).
[64]A. Schwabedissen, E. C. Benck, and J. R. Roberts, "Langmuir probe measurements in an inductively coupled plasma source," Phys. Rev. E **55**, 3450 (1997).
[65]M. Magarotto, P. De Carlo, G. Mansutti, F. J. Bosi, N. E. Buris, A.-D. Capobianco, and D. Pavarin, "Numerical suite for gaseous plasma antennas simulation," IEEE Trans. Plasma Sci. **49**, 285–297 (2021).
[66]P. De Carlo, M. Magarotto, G. Mansutti, S. Boscolo, A.-D. Capobianco, and D. Pavarin, "Experimental characterization of a plasma dipole in the UHF band," in IEEE Antennas and Wireless Propagation Letters, 2021.
[67]P. De Carlo, M. Magarotto, G. Mansutti, A. Selmo, A.-D. Capobianco, and D. Pavarin, "Feasibility study of a novel class of plasma antennas for SatCom navigation systems," Acta Astronaut. **178**, 846–853 (2021).
[68]A. Daykin-Iliopoulos, F. Bosi, F. Coccaro, M. Magarotto, A. Papadimopoulos, P. De Carlo, C. Dobranszki, I. Golosnoy, and S. Gabriel, "Characterisation of a thermionic plasma source apparatus for high-density gaseous plasma antenna applications," Plasma Sources Sci. Technol. **29**, 115002 (2020).
[69]G. Mansutti, P. De Carlo, M. A. Hannan, F. Boulos, P. Rocca, A.-D. Capobianco, M. Magarotto, and A. Tuozzi, "Modeling and design of a plasma-based transmitarray with beam scanning capabilities," Results Phys. **16**, 102923 (2020).